Contents lists available at SciOpen

Food Science and Human Wellness

journal homepage: https://www.sciopen.com/journal/2097-0765

China Food Publishing Co.

Polysaccharides from large leaf yellow tea activates the LXRα-ABCA1/ABCG1 pathway to ameliorate type 2 diabetes by regulating gut microbiota

Hao Chen[a,1], Xinxin Pei[a,1], Zhuang Wang[a,1], Jielin Chen[a], Kaili Xuan[a], Lei Gong[a], Xinyu Zhou[c], Yijun Wang[b,*], Yuzhe Huang[a,*], Yan Chen[a,*]

[a] *Key Laboratory of Ecological Engineering and Biotechnology of Anhui Province, School of Life Sciences and Medical Engineering, Anhui University, Hefei 230601, China*
[b] *National Key Laboratory for Tea Plant Germplasm Innovation and Resource Utilization, Anhui Agricultural University, Hefei 230036, China*
[c] *Fugong Yuanlveda Puluo Tea Industry Co., Ltd., Nujiang 673100, China*

ARTICLE INFO

Article history:
Received 10 May 2024
Received in revised form 29 July 2024
Accepted 1 November 2024

Keywords:
Lachnospiraceae bacterium
LXR*α*-ABCA1/ABCG1 signaling pathway
Type 2 diabetes mellitus
Large leaf yellow tea polysaccharide

ABSTRACT

Type 2 diabetes mellitus (T2DM) is a multifaceted metabolic condition characterized by chronic hyperglycemia (elevated blood sugar levels) and insulin resistance (IR). We have isolated a new homogeneous polysaccharide, LYTP-3 (7.22 × 10^5 Da), with anti-diabetic activity, from large leaf yellow tea (LYT) by biological activity-guided sequential separation and activity evaluation. Using a T2DM mouse model, we demonstrate that oral administration of LYTP-3 could reduce blood lipid levels, alleviate hyperglycemia and glucose tolerance, and inhibit IR. LYTP-3 ameliorated T2DM treatment by activating the liver X receptor alpha (LXRα)-ATP-binding cassette (ABC) transporter (LXRα-ABCA1/ABCG1) signaling pathway, which is regulated by the gut microbiota. The strain Lachnospiraceae bacterium A4 is potentially the key to this improvement. Additionally, we have solved the molecular structure of LYTP-3 using nuclear magnetic resonance (NMR), and methylation analyses. The main backbone of LYTP-3 consists of 1,2,4-*α*-*L*-Rha*p*, 1,4-*α*-*D*-Gal*p*, 1,6-*α*-*D*-Glc*p*, with branches of 1,4-*β*-*D*-Gal*p*, 1,6-*β*-*D*-GalpA, 1,3,6-*β*-*D*-Man*p*, 1,2-*α*-*L*-Rha*p*, T-*β*-Man*p*, and T-*β*-Gal*p*. The findings of this study suggest that LYTP-3 may serve as a potential gut microbiota modulator in the treatment of T2DM.

1. Introduction

In 2021, approximately 529 million adults worldwide were living with diabetes, and projections suggest that by 2050, this number could increase dramatically to 1.31 billion[1]. Diabetes caused 37.8 million years of life lost due to premature death and 41.4 million years of life lost due to disability, of which 95.4% are due to type 2 diabetes mellitus (T2DM). Adults with T2DM face significantly increased risks of cardiovascular disease (CVD), other comorbid conditions, and premature death. Apart from CVD, persistent hyperglycemia due to T2DM can cause a variety of complications including diabetic foot and diabetic retinopathy[2-3]. Diabetes prevention and treatment, particularly T2DM, have emerged as global issues. In addition to having side effects, currently prescribed hypoglycemic drugs are unable to effectively treat numerous symptoms of lipid and glucose metabolism in patients with diabetes[4-5]. Consequently, finding non-toxic, natural medications that can effectively treat T2DM is becoming crucial.

Polysaccharides, the complex carbohydrates, are natural prebiotics that support the growth and metabolism of gut microbiota[6].

[1] These authors contributed equally to the work and should be regarded as co-first authors.

* Corresponding author at: School of Life Sciences and Medical Engineering, Anhui University, Hefei 230601, China.
E-mail address: chenyan@ahu.edu.cn (Y. Chen); pfhuangyz@163.com (Y.Z. Huang)

Peer review under responsibility of Beijing Academy of Food Sciences.

SciOpen Publishing services by Tsinghua University Press

http://doi.org/10.26599/FSHW.2024.9250438

In turn, the gut microbiota plays a crucial role in breaking down polysaccharide, to produce beneficial metabolites that can significantly impact insulin resistance (IR) and energy metabolism, ultimately affecting the onset and progression of T2DM[7]. Polysaccharides have been shown to ameliorate T2DM by regulating gut microbes[8]. Crude polysaccharides of *Codonopsis pilosula*, a traditional medicinal herb, was shown to ameliorate T2DM by modulating the gut microbiome in a high-fat diet and streptozotocin-induced mouse model of T2DM[9]. Furthermore, polysaccharides from small black soybeans alleviate T2DM by modulating the gut microbiota. Thus, gut microbiota is attracting attention as an important target for the treatment of T2DM[10].

Large leaf yellow tea (LYT), is a distinctive type of tea cultivated in the Ta-pieh Mountains of China, and unlike other common teas, it is made from older leaves harvested during the summer and autumn seasons. This unique tea has been gaining attention because of its health benefits. Studies have shown that LYT reduces blood glucose levels and improves glucose tolerance and IR[11]. However, the major component responsible for the hypoglycemic activity of LYT extract remains unclear. LYT polysaccharides (LYTP) are one of the main functional components of LYT, and have been shown to possess anti-inflammatory[12], antioxidant[13], hepato-protective[14], and macrophage polarization-regulating activities[15]. However, reports on the effects of LYTP on T2DM are lacking.

In the present study, we purified 3 homogeneous polysaccharides (LYTP-1, LYTP-2, and LYTP-3) from LYT, and investigated their potential for reducing blood glucose and lipid levels. We found that LYTP-3 significantly ameliorated T2DM. We also identified the key bacterial strains in LYTP-3 that improved T2DM, and studied the involved molecular mechanisms through metagenomic sequencing and Spearman analysis.

2. Materials and methods

2.1 Materials and reagents

LYT was obtained from Hengda Biotechnology Co., Ltd. (Huoshan, Anhui, China). 1-Phenyl-3-methyl-5-pyrazolone (PMP) was purchased from Adamas-beta (Shanghai, China). DEAE-Sepharose FF was purchased from GE Healthcare (Chicago, IL, USA). Streptozotocin and dextran standard (CAS:9004-54-0, USA) were purchased from Sigma-Aldrich (St. Louis, MO, USA). Metformin (MET) hydrochloride and 7 standard monosaccharides (mannose (Man), rhamnose (Rha), glucuronic acid (GlcA), galacturonic acid (GaU), glucose (Glc), galactose (Gal), and arabinose (Ara)) were purchased from Aladdin Biochemical Technology Co. Ltd., (Shanghai, China). High-density lipoprotein (HDL-C), total cholesterol (TC), low-density lipoprotein (LDL-C), and triglycerides (TG) were purchased from Nanjing, China. Insulin (INS), glycated hemoglobin (HbA1c), and glucagon peptide-1 (GLP-1) were purchased from Ruixin Biotechnology (Fujian, China). Trifluoroacetic acid (TFA) was purchased from MacLean Biochemical Co., Ltd. (Shanghai, China). A glucose colorimetric assay kit was purchased from Invitrogen (Carlsbad, CA, USA). All chemicals and reagents used were of analytical grade.

2.2 Preparation of LYTP-3

The dried LYT is ground and sifted through an 80-mesh sieve. The material is then subjected to vacuum filtration. To remove fats, colors, and small molecular components, 95% ethanol is added to the dried and ground LYT. Subsequently, the residues are dried in a vacuum oven at 60 ℃ for 24. The pretreated LYT powder was extracted with HCl solution (0.01 mol/L, *m/V* = 1:20) for 1.5 h and the pH was adjusted to 7 using NaOH solution[16]. It was precipitated overnight with anhydrous ethanol at 4 °C in a ratio of 1:4, and the precipitate was collected[17]. After deproteination with Sevage reagent (trichloromethane/*n*-butanol, *V/V* = 4:1), the solution was dialyzed in 3 500 Da dialysis bags (MD 34, Solarbio, China) for 3 days and lyophilized (α 1–4 Lo plus, Christ, Germany) to obtain the crude polysaccharide (LYTP)[18]. LYTP solution (120 mg/mL) was loaded onto a DEAE-Sepharose FF column and eluted with different concentrations (0, 0.1, 0.2, and 0.3 mol/L) of 5 mL NaCl. The different polysaccharide components were collected using the phenol-sulfuric acid method[19], concentrated, dialyzed, and freeze-dried to obtain LYTP-1, LYTP-2, and LYTP-3.

2.3 Chemical composition and molecular weight distribution of LYTP-3

Using *D*-glucose as a standard, the total sugar content of each polysaccharide was calculated using the phenol-sulfuric acid method at 490 nm[19]. The uronic acid content of each polysaccharide was determined using the carbazole-sulfuric acid method at 530 nm[20], for which a calibration curve was generated using galacturonic acid as the standard. The protein content was determined using the Coomassie Brilliant Blue G-250 method at 595 nm with bovine serum albumin as the reference[21]. The total phenol content was determined using gallic acid as a standard[13].

The molecular weight of LYTP-3 was determined using high performance liquid chromatography (HPLC) combined with an evaporative light scattering detector (ELSD) on a TSK gel G6000PWXL column (7.8 mm × 300 mm, Tosoh, Japan). Double-distilled water was used as the mobile phase at a flow rate of 0.6 mL/min. The injection volume was 20 μL and the column temperature was 30 ℃[22].

2.4 Monosaccharide composition of LYTP-3

The monosaccharide composition of LYTP-3 was determined by modification of previously published methods[23]. Briefly, the monosaccharide composition of LYTP-3 was determined on a C_{18} column (4.6 mm × 250 mm, 5 μm, Tosoh, Japan) by HPLC 1260 system combined with 245 nm diode array detector (DAD). LYTP-3 (10 mg) containing trifluoroacetic acid (TFA, 2.5 mol/L, 5 mL) was placed in a test tube with a stopper, sealed with nitrogen, oil bathed at 110 ℃ for 5 h, and then appropriate volumes of methanol was added at 65 ℃ to remove TFA by rotary evaporation. After that, the hydrolyzed samples and standard monosaccharides derived from PMP were dissolved in 0.8 mL distilled water and mixed with PMP (0.5 mol/L, 0.5 mL) and sodium hydroxide solution (0.5 mol/L, 0.5 mL) at 70 ℃ for 1 h, and then neutralized with HCl solution (0.5 mol/L, 0.5 mL). Finally, chloroform was used for multiple extractions, the solution

filtered with 0.22 μm membrane, and the filtrate was injected into the column. The mobile phase consisted of ammonium acetate solution and acetonitrile. The column temperature was 30 ℃ and the flow rate was 1.0 mL/min.

2.5 Methylation and nuclear magnetic resonance (NMR) analysis of LYTP-3

LYTP-3 (40 mg) was pre-reduced with NaBD4. Then, the reduced sample was completely methylated with methyl iodide, hydrolyzed with formic acid and TFA (2 mol/L) at 110 ℃ for 10 h. Subsequently, the product was reduced using $NaBD_4$ and acetylated with pyridine and acetic anhydride. Methylated sugar alcohol acetate was analyzed by gas chromatography-mass spectrometry (GC-MS) (Agilent 7890A/5975C, USA), and a RTX-5MS chromatographic column was configured from 50 ℃ (hold for 7 min) to 320 ℃ (hold for 14 min) at a frequency of 10 ℃/min. High-purity (99.99%) helium was used as the carrier gas at a flow rate of 1.0 mL/min[18].

LYTP-3 (60 mg) was dissolved in D_2O (1.5 mL) and freeze dried. The sample was then re-dissolved in D_2O (0.6 mL), and the supernatant after centrifugation was transferred to a 5 mm NMR tube. Sodium 2,2-dimethyl-2-silylpentane-5-sulfonate (DSS) was used as the internal standard. The 1D (^1H, ^{13}C) and 2D (COSY, HSQC and HMBC) NMR spectra of LYTP-3 were recorded by JNM-ECZ600R digital FT-NMR spectrometer at 50 ℃[24].

2.6 Animal experiments

The 5 week-old male C57BL/6J mice were purchased from the Experimental Animal Center of Anhui Medical University (SCXK, Anhui 2022-004). The mice were housed in a monitored environment ((25 ± 1) ℃, 12-h light-dark cycle). The mice were acclimated to feeding for 7 days and were provided food and water *ad libitum* before the experiment began. All animal experiments were approved by the Experimental Animal Ethics Committee of Anhui University (Approval No.: 2020-005).

For determining the active components of LYTP, high-fat diet (HFD; D12492, 60% calories from fat, Research Diets, Inc., USA) combined with streptozotocin (STZ; 40 mg/kg, dissolved in 0.1 mol/L citrate buffer, pH 4.5 administered for 5 days)-induced T2DM mice after a 6-week HFD were used. All mice were randomly divided into normal control (NC), model (DM), metformin (MET), LYTP, LYTP-1, LYTP-2 and LYTP-3 groups. Mice were treated with phosphate buffered saline (PBS), metformin (200 mg/kg·day), LYTP, LYTP-1, LYTP-2, or LYTP-3(400 mg/kg·day)[10]. There were 8 mice in each group.

For the LYTP-3 efficiency assay in HFD mice with STZ-induced T2DM were treated with PBS, MET, low-dose LYTP-3 (LLYTP-3, 100 mg/kg), middle-dose LYTP-3 (MLYTP-3, 200 mg/kg), or high-dose LYTP-3 (HLYTP-3, 400 mg/kg).

For gut microbiota-dependent assay in HFD combined with STZ-induced T2DM mice, the microbiota donor mice were treated with 400 mg/kg·day LYTP-3 or PBS for 4 weeks, followed by daily collection of feces. 100 mg of feces were resuspended in 1 mL of sterile anaerobic PBS and centrifuged (500 × *g*, 4 °C for 1 min). After 6 weeks of HFD and 5 days of STZ treatment, mice were treated with antibiotic (Ab) cocktails (ampicillin, 200 mg/kg; metronidazole, 200 mg/kg; vancomycin, 100 mg/kg; and neomycin sulfate, 200 mg/kg) by daily gavage for 7 days, followed by a daily oral gavage of 200 μL suspension for 4 weeks (Fig. S1)[7].

2.7 Metabolic analysis

Fasting blood glucose (FBG) levels were measured at weeks 8, 9, 10, 11, and 12. At the end of the experiment, the mice were euthanized and blood and liver tissues were collected for biochemical analysis. Oral glucose tolerance test (OGTT) was performed on all mice during the last week of the experiment. The animals were fed glucose solution (2 g/kg body weight). Blood glucose levels were measured at 0, 30, 60, 90, 120, and 180 min after glucose administration using (Accu-Chek meter). The area under the curve (AUC) was calculated using the trapezoidal rule to quantify the OGTT results[25].

2.8 Biochemical analysis

TG, HDL-C, LDL-C, TC, HbA1c, GLP-1, and liver glycogen contents were measured according to the manufacturer's instructions (Nanjing Jiancheng Institute of Biotechnology, Nanjing, China). Serum fasting insulin (FINS) levels were measured according to the manufacturer's instructions. The homeostasis model assessment (HOMA) was performed using FBG and insulin levels[26]. The HOMA-IR was calculated using the following formula:

$$\text{HOMA-IR} = \frac{\text{FINS (mIU/L)} \times \text{FBG (mmol/L)}}{22.5}$$

2.9 Histological analysis

Mouse liver tissues were fixed overnight in 4% paraformaldehyde. Paraffin-embedded sections were stained with hematoxylin and eosin (H&E) and periodic acid-Schiff (PAS). Frozen sections were stained with Oil red O. Images were captured using an IX73 Olympus microscope[7].

2.10 Macrogenomic analysis

Total sample microbial DNA was extracted using a DNA extraction kit (QIAamp® Fast DNA Stool Mini Kit (Qiagen, Hilden, Germany). DNA fragmentation was performed using an S220 focused ultrasonicator (Covaris, USA) and purification was performed using Agencourt AMPure XP beads (Beckman Coulter Co., USA). Library construction was performed using the TruSeq Nano DNA LT Sample Preparation Kit (Illumina, San Diego, CA, USA). The library was sequenced using the Illumina NovaSeq 6000 sequencing platform, and 150 bp double-ended reads were generated[27]. The taxonomy of the species was obtained from the corresponding taxonomy database of the NR Library, and the abundance of the species was calculated using the corresponding gene abundance. To construct the abundance profile at the corresponding taxonomic level, abundance statistics were performed at each level of the domain, kingdom, phylum, class, order, family, genus, and species.

2.11 Western blotting analysis

Liver tissues (90 mg) were homogenized, lysed, and then centrifuged at 13 400 × *g* and 4 ℃ for 10 min. The resulting supernatant was collected for determination of protein content.

Proteins were then separated by electrophoresis on a 12% sodium dodecyl sulfate-polyacrylamide gel and transferred to 0.45 μm polyvinylidene fluoride membranes. These membranes were incubated in 5% skim milk in tris-buffered saline with Tween-20 (TBST), followed by overnight probing at 4 ℃ with primary antibodies targeting nuclear factor liver X receptor alpha (LXRα), ATP-binding cassette transporter (ABC)A1, ABCG1, and glyceraldehyde-3-phosphate dehydrogenase (GAPDH). After washing 5 times with TBST, the membranes were treated with horseradish peroxidase-labeled goat anti-rabbit IgG. Protein bands were detected by enhanced chemiluminescence and captured using a gel imaging system. The band density was normalized to that of GAPDH and analyzed using ImageJ 1.53k software.

2.12 Statistical analysis

Data are expressed as mean ± standard deviation (SD). All statistical analyses were performed using GraphPad Prism version 7 (GraphPad Software, San Diego, CA, USA). Statistical significance was determined using unpaired two-tailed Student's *t*-test. DIAMOND (v0.9.10.111) software was used to compare and annotate the representative sequence (amino acid sequence) of the gene set with the NR database, Kyoto Encyclopedia of Genes and Genomes (KEGG), Clusters of Orthologous Groups (COG), SWISSPROT, Gene Ontology (GO), and other databases. Using the R package (version 4.1.2), the species abundance spectrum or functional abundance spectrum was analyzed by principal component analysis (PCoA) and plotted, and the results of the PCoA and non-metric multidimensional scaling (NMDS) equidistance matrices were calculated and plotted. Based on the R-package, analysis of variance (ANOVA)/Kruskal-Wallis/*t*-test/Wilcoxon tests were used to analyze the differences. Linear discriminant analysis Effect Size (LEfSe) was used to identify and characterize differences in species abundance.

3. Results

3.1 LYTP-3 reduces blood glucose and lipid in T2DM mice

To identify the active ingredients of LYTP that are responsible for the anti-diabetic effect, LYTP-1 (1.29×10^4 Da), LYTP-2 (2.09×10^4 Da), and LYTP-3 (7.22×10^5 Da) were identified and isolated from LYTP. The chemical compositions and yields of LYTP-1, LYTP-2, and LYTP-3 are listed in Table S1. A T2DM model was established using HFD combined with STZ treatment. We observed that the level of blood glucose and lipids in the DM group were significantly higher than those in the NC group (Fig. 1). The FBG, OGTT, FINS, TC, and TG levels in the LYTP-3 group were the lowest among the 3 homogeneous LYTP polysaccharides. These results indicated that the anti-diabetic activity of LYTP mainly comes from LYTP-3.

3.2 LYTP-3 restores the disorder of glucose and lipid metabolism

The body weight of T2DM mice decreased significantly from the 6th week, but supplementation with LYTP effectively restores the body weight (Fig. 2a). As shown in Table S4, LYTP-3 reduced the FBG levels in diabetic mice. The OGTT showed that LYTP-3 effectively reduced the AUC index and enhanced glucose tolerance (Figs. 2b-c). FINS and HOMA-IR levels were also significantly lower in LYTP-3-treated mice than in the diabetic mice (Figs. 2e-f). Compared to the DM group, HbA1c levels of the MLYTP-3 and HLYTP-3 groups decreased, whereas the HbA1c level of the LLYTP-3 group was not

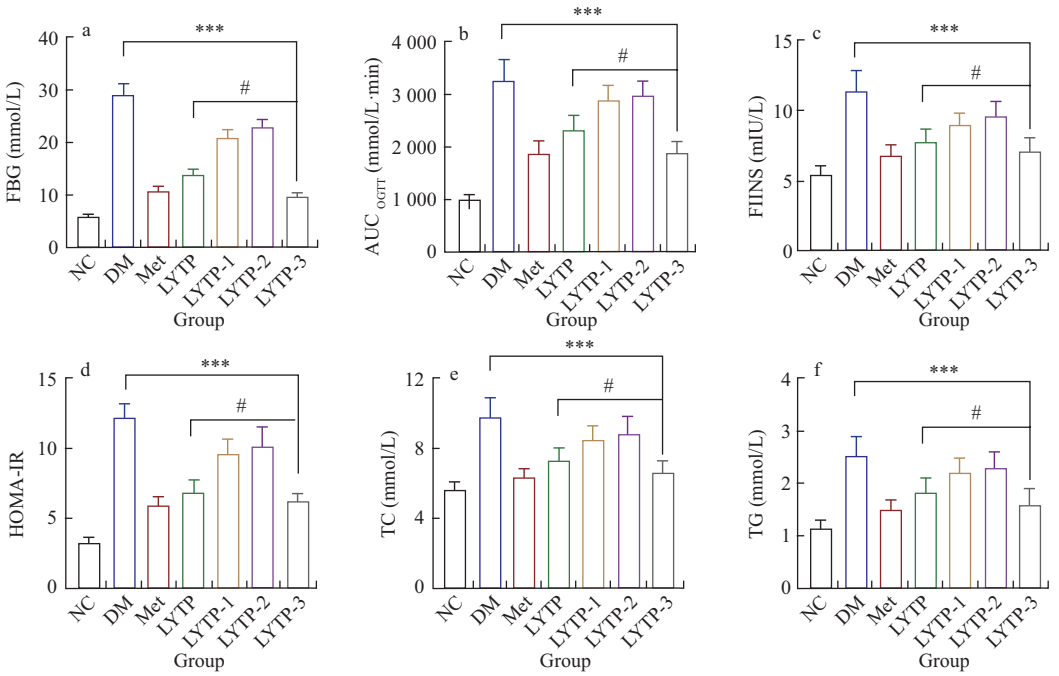

Fig. 1 LYTP-3 reduces blood glucose and blood lipid in T2DM mice. (a) FBG, (b) AUC_{OGTT}, (c) FINS, (d)HOMA-IR, (e) TC, and (f) TG. Data were presented as means ± SD ($n = 8$). ***$P < 0.001$ *vs*. DM group; $^{\#}P < 0.05$ *vs*. LYPT group. Data are pooled from 3 independent experiments.

statistically significant (Fig. 2d). Consistent with the improvement in glucose metabolism, LYTP-3 regulated abnormal lipid metabolism by decreasing TC, TG, and LDL-C levels and increasing HDL-C levels (Figs. 2i-l). LYTP-3 supplementation significantly ameliorated obvious lesions, extensive vacuolization, accumulation of microbubble fat, and reduction in liver glycogen levels in diabetic mice as observed by H&E (Fig. 3a), Oil red O (Fig. 3b), and PAS (Fig. 3c) staining. These data provide cumulative evidence that LYTP-3 effectively improves glucose and lipid metabolism disorders in T2DM mice.

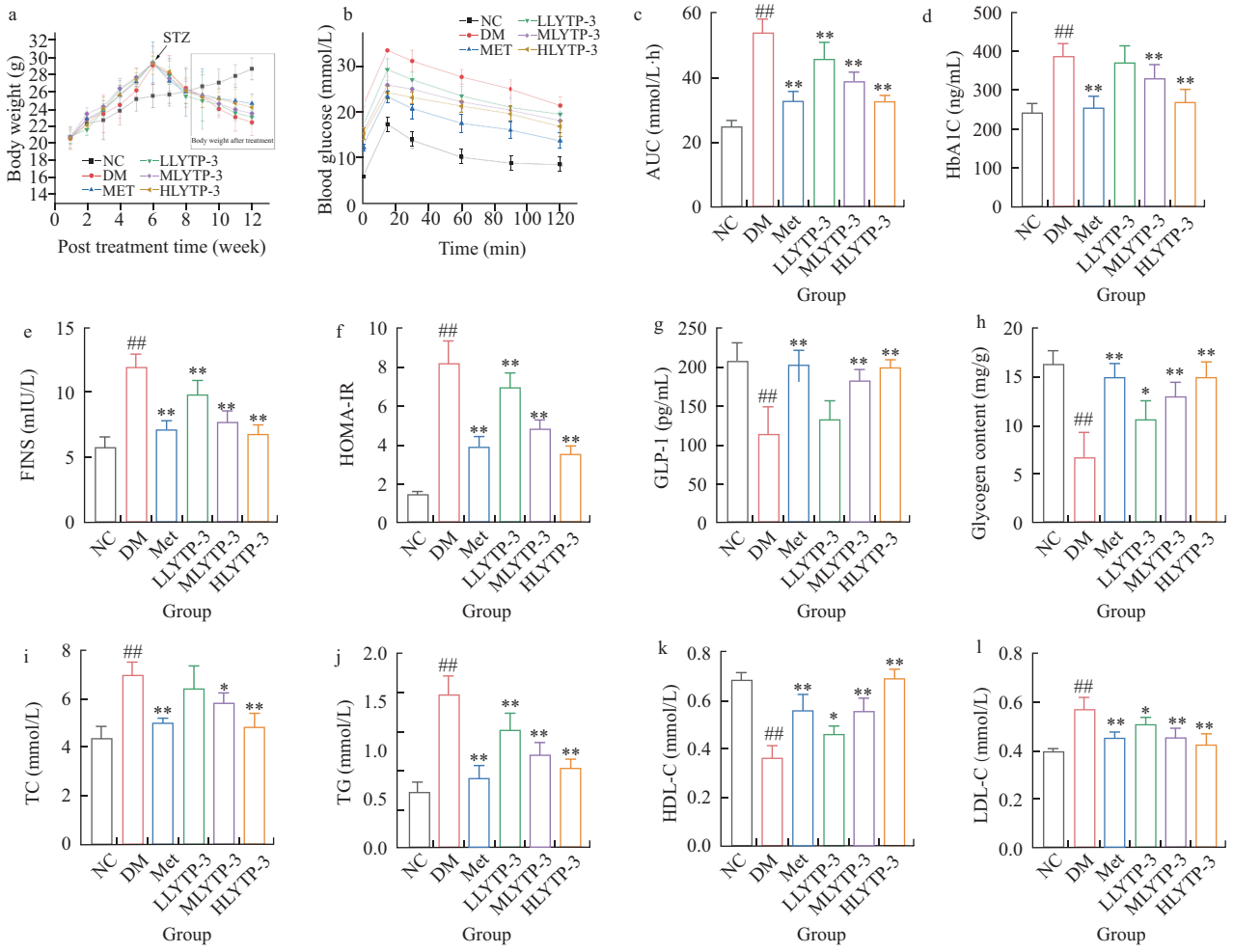

Fig. 2 Effect of LYTP-3 on glucose and lipid metabolism in T2DM mice. (a) Body weight, (b) oral glucose tolerance test, (c) AUC, (d)HbA1C, (e) FINS, (f) HOMR-IR, (g) GLP-1, (h) glycogen content, (i) TC, (j) TG, (k)HDL-C, and (l) LDL-C. Data were presented as means ± SD. $^{*}P < 0.05$, $^{**}P < 0.01$, *vs*. DM group. $^{\#}P < 0.01$ *vs*. NC group. Data are pooled from three independent experiments.

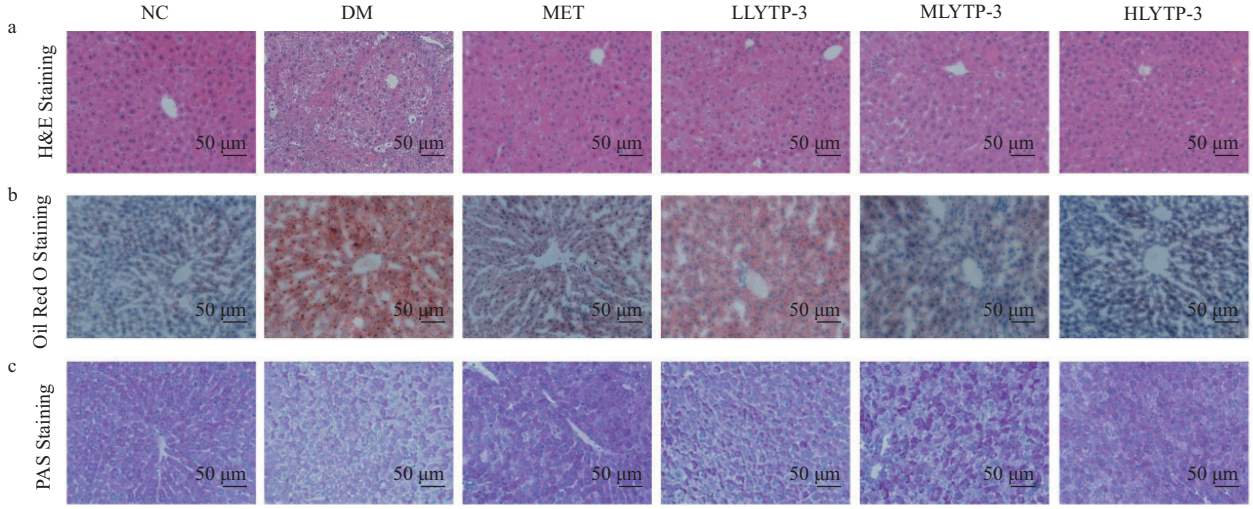

Fig. 3 Histopathological analysis of anti-T2DM effects from LYTP-3. (a) H&E staining, (b) Oil red O staining, and (c) PAS staining. All images were captured at 200× magnification.

3.3 *LYTP-3 could modulate the gut microbiota*

Gut bacteria and their metabolites can influence glucose and lipid metabolisms in multiple ways[28-29]. Previous studies have demonstrated that dysbiosis of the gut microbiota is inextricably linked to the development and progression of T2DM[30-31]. To study the effect of LYTP-3 on the composition of the intestinal flora in diabetic mice, we performed metagenomic sequencing of intestinal microorganisms. LYTP-3 significantly increased the diversity and richness of the taxa of the gut microbiota in T2DM mice (Figs. 4a-c) and the composition of the gut microbiota was close to that of the NC group (Fig. 4d). Regarding species differences, the DM group had higher *Clostridium* sp. CAG:557, Lachnospiaceae bacterium and bacterium J10(2018), whereas those of Lachnospiraceae_bacterium_A4 and bacterium_0.1xD8-71 were lower than those in the NC and LYTP-3 groups (Figs. 4e-g). The LYTP-3 group was characterized by enriched Bacteroidales bacterium, Muribaculaceae and Lachnospiraceae_bacterium_A4, whereas Clostridium_sp_CAG:557,

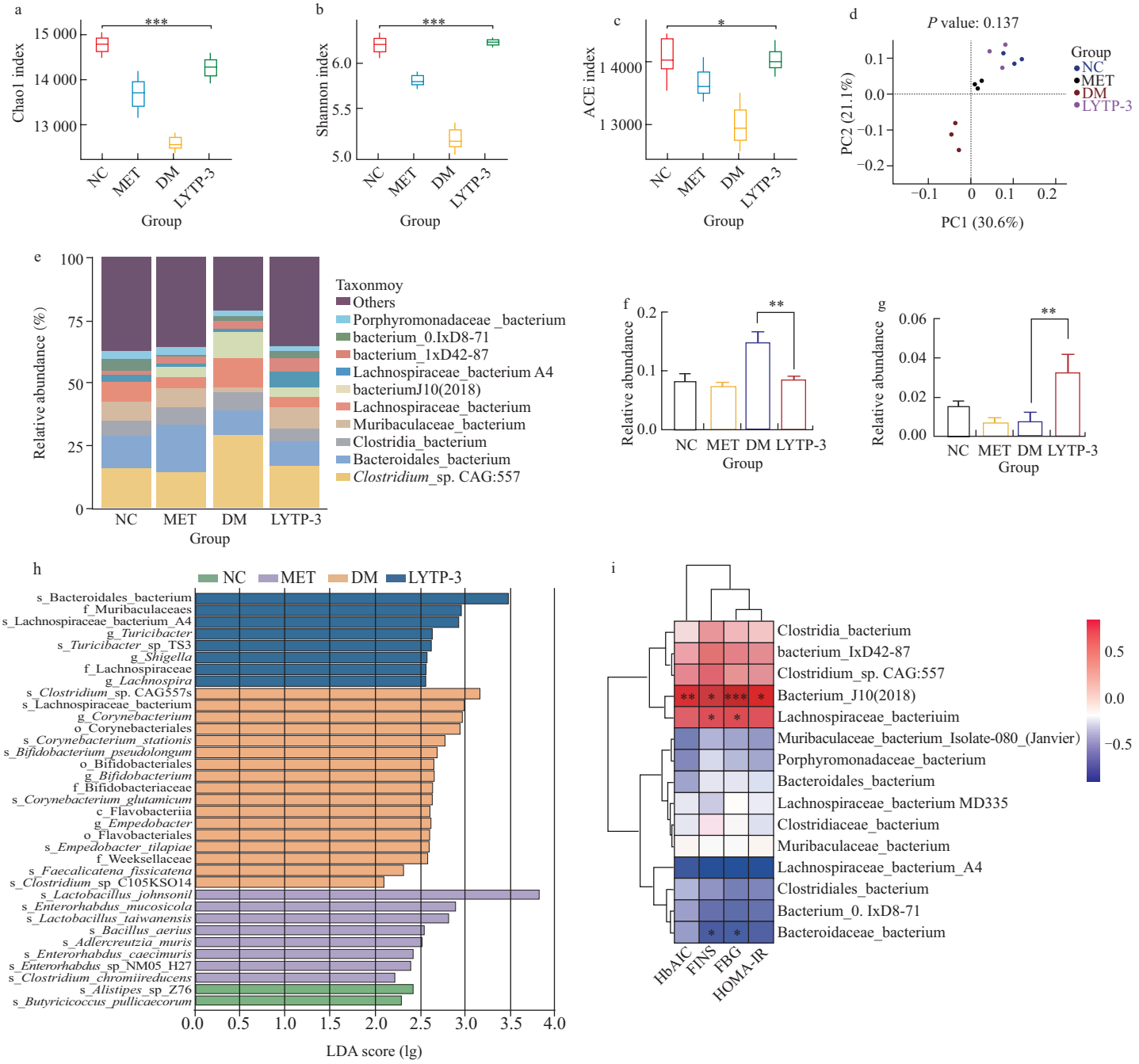

Fig. 4 Effect of LYTP-3 on gut microbiota. α-Diversity indexes in different groups as indicated by the (a) Chao1, (b) Shannon, and (c) ACE indexes. (d) Principal coordinate analysis (PCoA) analysis. (e) Relative abundance of bacteria at the species level in different groups. The relative abundance of (f) *Clostridium*_sp_CAG:557 and (g) Lachnospiraceae_bacterium_A4. (h) LDA score of different groups. (i) Spearman correlations (two-tailed Spearman's rank test) between the species-level abundance and T2DM phenotypes. (j) Heat map of metabolites involved in the significantly changed metabolic pathways. (k) Spearman correlations (two-tailed Spearman's rank test) analysis between the ABC transporters and T2DM phenotypes. The color represents positive (red) or negative (blue) correlations and FDRs are denoted: *FDR < 0.05; **FDR < 0.01; ***FDR < 0.001.

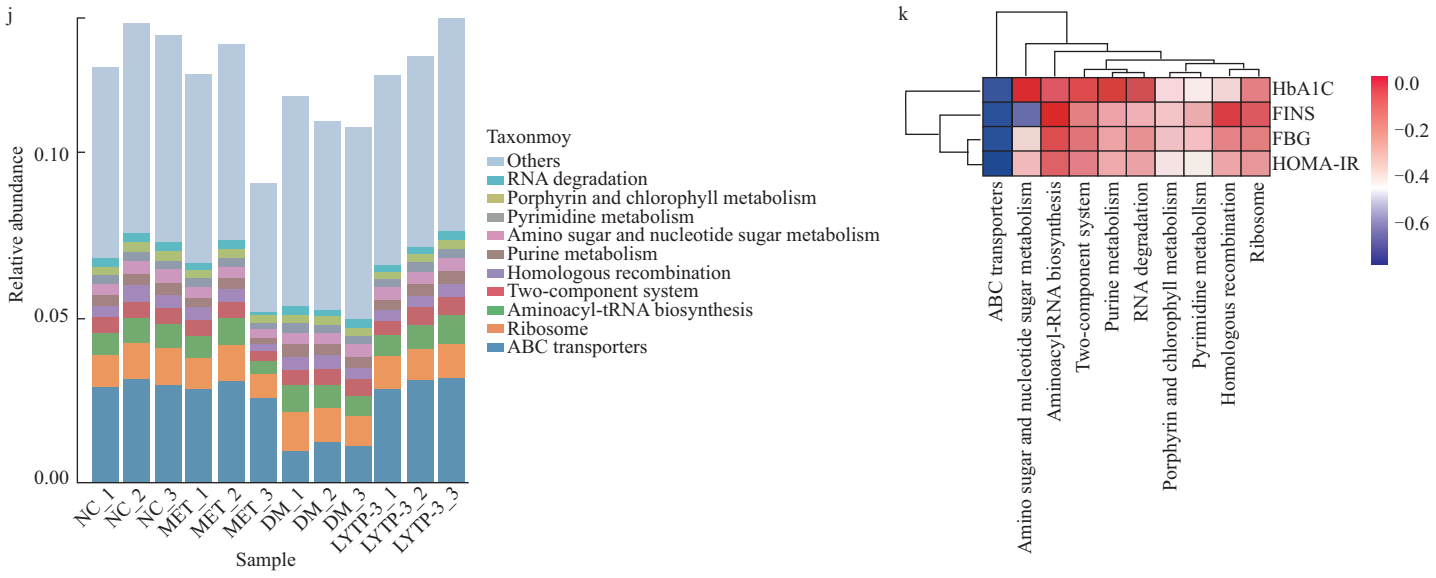

Fig. 4 (*Continued*)

Lachnospiraceae_bacterium_A4, Corynebacterium and Corynebacteriales were the dominant bacteria in the DM group according to linear discriminant analysis (LDA) coupled with LEfSe (Fig. 4h). Lachnospiraceae_bacterium_A4 was negatively correlated with HbA1c, FINS, FBG, and HOMA-IR (Fig. 4i). These results indicate that Lachnospiraceae_bacterium_A4 has the potential to serve as a strain that can indicate the severity of T2DM phenotypes.

3.4 Gut microbiota is responsible for alleviating T2DM through LYTP-3

Our results proved that LYTP-3 significantly improves the composition of the gut microbiota in T2DM mice. To investigate whether LYTP-3 could alleviate T2DM by remodeling the intestinal microenvironment, we administered antibiotics to mice (Fig. S1). As

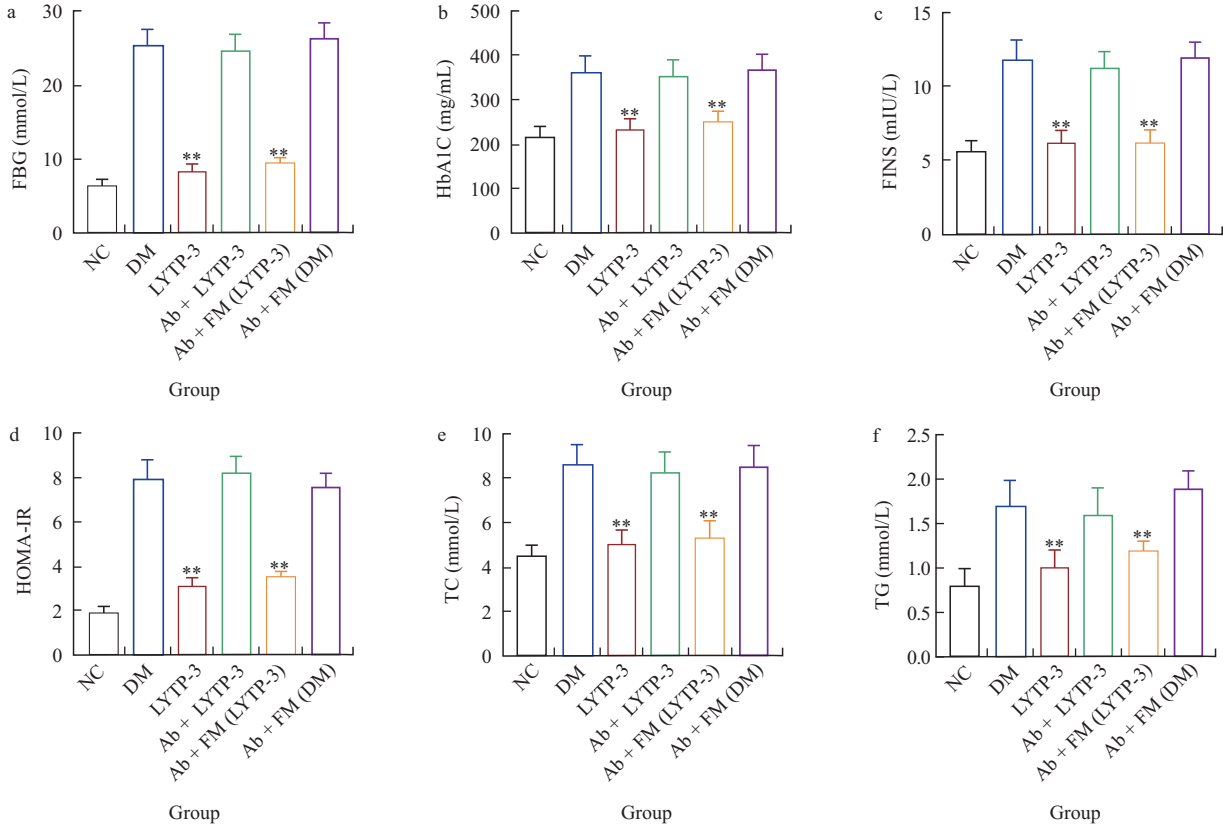

Fig. 5 The microbial flora of LYTP-3-treated mice could effectively reduce blood sugar and blood lipid. (a) FBG, (b) HbA1c, (c) FINS, (d) HOMA-IR, (e) TC, (f) TG. (g) Relative abundance of bacteria at the species level in different groups and (h) Spearman correlations (two-tailed Spearman'srank test) between the species leve labundance and expression of key regulatory proteins in LXRα-ABCA1/ABCG1 pathway. Data were presented as means ± SD ($n = 8$). $^{**}P < 0.01$ *vs*. DM group.

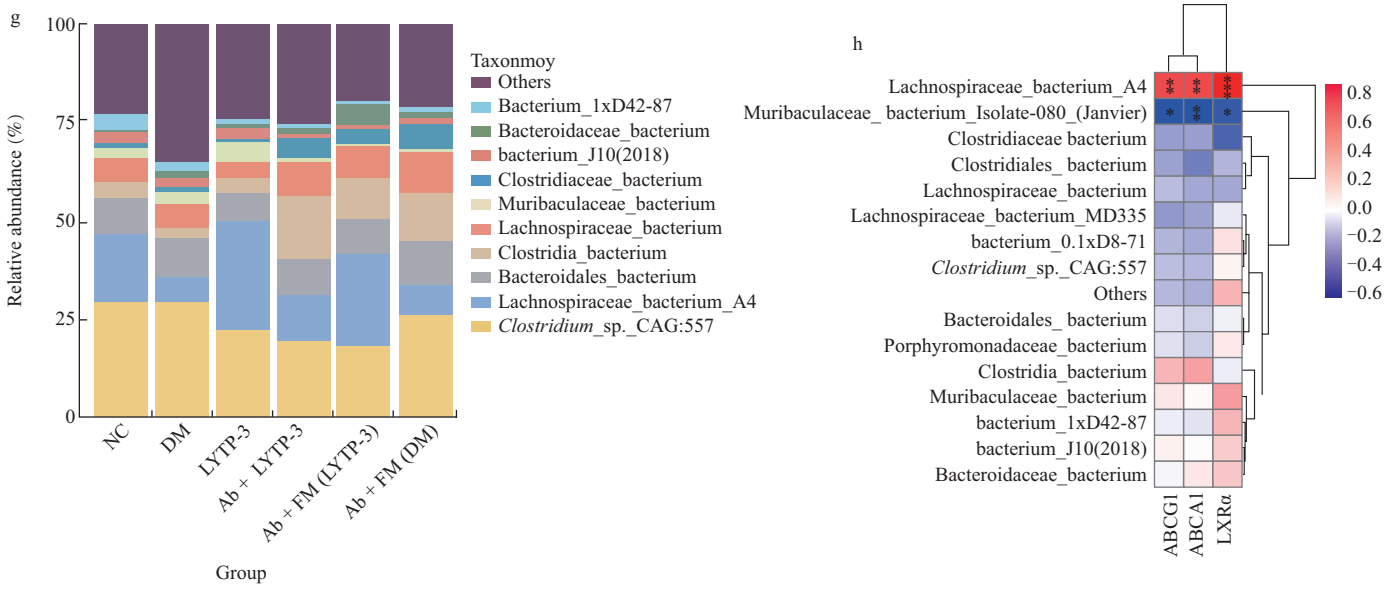

Fig. 5 (*Continued*)

shown in Fig. 5, the FBG, HbA1C, FINS, HOMA-IR, TG, and TC levels in the Ab + LYTP-3 group were not significantly different from those in the DM group. To further prove that the alleviation of T2DM by LYTP-3 was microbially dependent, we transplanted the microbial flora of LYTP-3-treated mice into DM mice. The FBG, HbA1C, FINS, HOMA-IR, TG, and TC levels in the Ab + FM (LYTP-3) group were lower than those in the DM group; however, there was no significant difference in the Ab + FM (DM) group (Fig. 5). Notably, the abundance of Lachnospiraceae_bacterium_A4 in the Ab + FM (LYTP-3) group was significantly higher than that in the Ab + FM (DM) group (Fig. 5g). These findings were consistent with the hypothesis that the alleviation of T2DM by LYTP-3 is microbiota-dependent.

3.5 LYTP-3 promotes cholesterol excretion by activating LXRα-ABCA1/ABCG1 pathway

The metabolic functions of the intestinal flora were predicted based on the KEGG database. The carbohydrate metabolism pathway was the most favorable among the 11 metabolic systems shown in Fig. S2 (level 2). As shown in Fig. 4j, we noted a significant decrease in the abundance of ABC transporters in the DM group compared to the NC group. However, treatment with LYTP-3 effectively reversed this effect (level 3). Additionally, we observed a negative correlation between the abundance of ABC transporters and the levels of HbA1c, FINS, FBG, and HOMA-IR (Fig. 4k).

We hypothesized that LYTP-3 ameliorates T2DM by increasing the abundance of Lachnospiraceae_bacterium_A4, thereby activating pathways associated with ABC transporters. Studies have indicated that the expression of ABC transport proteins (including ABCA1 and ABCG1), which facilitate the efflux of cholesterol from cells, is suppressed under high glucose conditions. Our findings demonstrated that the expression levels of ABCA1/ABCG1 in the model group were significantly lower than those in the control group (Figs. 6a-c). Metformin treatment did not significantly alter the expression levels of ABCA1/ABCG1. In contrast, both the LYTP-3 and Ab + FM (LYTP-3) groups exhibited a significant increase in ABCA1/ABCG1 expression compared to the model, Ab + LYTP-3, and Ab + FM (DM) groups (Figs. 6a-c). Furthermore, through Western blotting and immunohistochemistry analysis, we assessed the expression levels of LXRα, a key regulatory factor upstream of the ABCA1/ABCG1 pathway. We observed that LYTP-3 significantly upregulated the expression of LXRα in the presence of intestinal microbiota (Figs. 6a and d). Intriguingly, the abundance of Lachnospiraceae_bacterium_A4 showed a significant positive correlation with the expression levels of LXRα-ABCA1/ABCG1 (Fig. 5h). These findings substantiate our hypothesis that LYTP-3 enhances T2DM management by activating the LXRα-ABCA1/ABCG1 pathway, which promotes cholesterol efflux, a process critically dependent on the intestinal microbiota, particularly Lachnospiraceae_bacterium_A4.

3.6 Structural analysis of LYTP-3

To advance our understanding of the molecular mechanisms underlying the effectiveness of LYTP-3 in improving T2DM treatment, we used infrared spectroscopy, NMR, and methylation analyses to predict its molecular structure.

3.6.1 Chemical constituents of LYTP-3

The HPLC chromatogram of LYTP-3 is shown in Fig. 7b. The Polymer dispersity index (PDI) of LYTP-3 was 1.021, indicating that LYTP-3 is a homogeneous polysaccharide (Table S2). The molecular weight of LYTP-3 was calculated to be 7.22×10^5 Da. The monosaccharide mixture standard diagram and monosaccharide composition diagram of LYTP-3 are shown in Figs. 7c-d. There are six monosaccharides: mannose, rhamnose, galacturonic acid, glucose, galactose, and arabinose (molar ratios of 1:0.2:4.34:2.14:1.10:2.28).

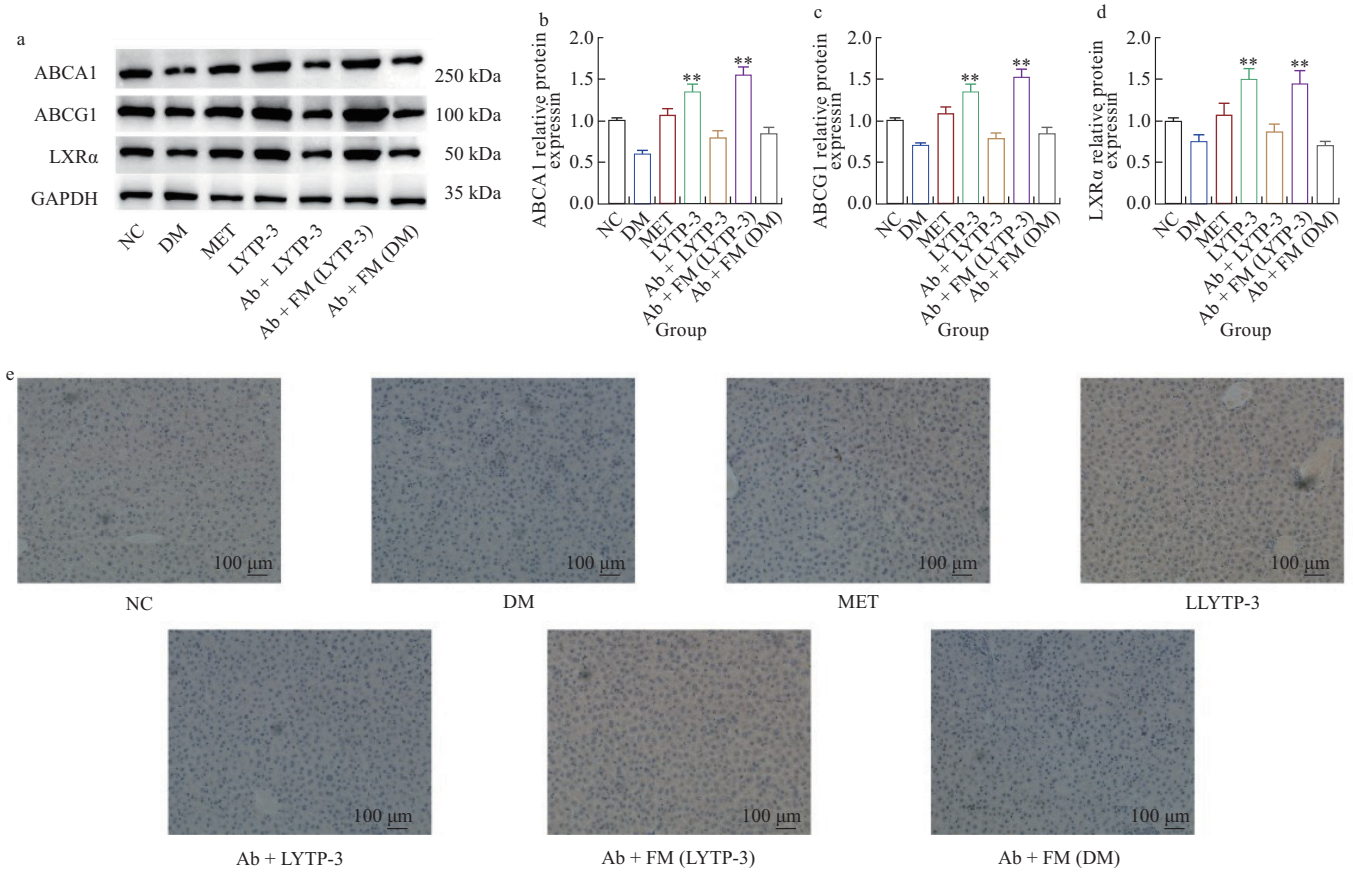

Fig. 6 LYTP-3 activated LXRα-ABCA1/ABCG1 pathway Effect of LYTP-3 on the expression level of LXRα, ABCA1 and ABCG1. (a) Western blot analysis of LXRα, ABCA1, ABCG1 and GAPDH. (b-d) The relative intensity is normalized to that of GAPDH. (e) Immunohistochemical staining of LXRα in liver tissues. $^{**}P < 0.01$, *vs*. DM group. All images were captured at 100× magnification. Data are pooled from 3 independent experiments.

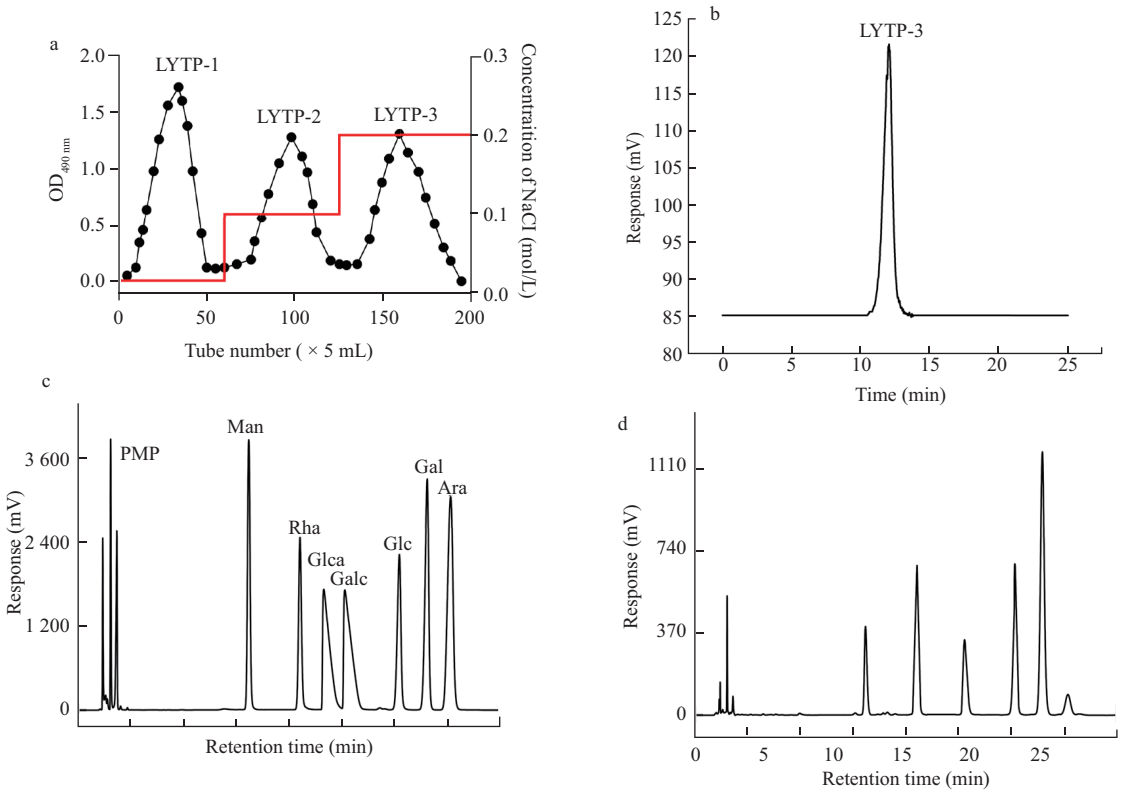

Fig. 7 Elution curves of isolation of (a) LYTPs, (b) HPLC diagrams of LYTP-3, chromatograms of PMP derivatives of (c) mixed monosaccharide standards and (d) LYTP-3.

Table 1
Methylation analysis and type of linkage of LYTP-3.

Methylated sugars	Linkages	Retention time (min)	Molar percentage	Mass fragments (*m/z*)
3,4-Me2-Rha*p*	2-linked Rha*p*	7.68	4.45	57, 71, 89, 100, 115, 130, 131, 190
2,3,4,6-Me4-Man*p*	T-Man*p*	8.16	4.13	71, 87, 102, 118, 129, 145, 162
2,3,4,6-Me4-Gal*p*	T-Gal*p*	8.44	15.16	71, 87, 102, 118, 129, 145, 161, 205
3-Me-Rha*p*	1,2,4-linked Rha*p*	8.77	16.88	88, 101, 130, 143, 190, 203
2,3,6-Me3-Gal*p*	1,4-linked Gal*p*	9.28	17.28	71, 87, 99, 102, 113, 118, 131, 173, 233
2,3,6-Me3-Gal*p*A	1,4-linked Gal*p*A	9.28	4.38	75, 99, 102, 117, 129, 159, 173, 233
2,3,4-Me3-Glc*p*	1,6-linked Glc*p*	9.52	19.66	71, 87, 99, 102, 118, 129, 159, 162, 173, 189
2,3,4-Me3-Gal*p*	1,6-linked Gal*p*	9.9	2.91	87, 99, 102, 118, 129, 159, 162, 189
2,3,4-Me3-Gal*p*A	1,6-linked Gal*p*A	9.9	7.18	73, 99, 117, 143, 159, 162, 173, 203, 233
4-Me-Glc*p*	1,3,6-linked Glc*p*	10.56	2.75	87, 102, 118, 129, 139, 160, 189,
4-Me-Man*p*	1,3,6-linked Man*p*	10.86	5.19	87, 101, 118, 129, 139, 160, 174, 189

3.6.2 Methylation analysis of LYTP-3

Methylation analysis was conducted to reveal the glycosidic linkages in LYTP-3 (Table 1). By comparing with the Complex Carbohydrate Research Center (CCRC) spectral database (https://www.ccrc.uga.edu/specdb/ms/pmaa/pframe.html), 11 main glycosidic bonds were deduced from the polysaccharide component LYTP-3, namely, 1,2-Rha*p*, T-Man*p*, T-Gal*p*,1,2,4-Rha*p*, 1,4-Gal*p*, 1,4-Gal*p*A, 1,6-Glc*p*, 1,6-Gal*p*, 1,6-Gal*p*A, 1,3,6-Glc*p*, and 1,3,6-Man*p*, with the molar percentage of 4.45:4.13:15.16:16.88:17.28:4.38:19.66:2.91:7.18:2.75:5.19[15,18,32]. Glycosidic residues of arabinose were not found, which may be due to the low sugar residue content.

3.6.3 NMR analysis of LYTP-3

The structural characteristics of LYTP-3 were further analyzed using ^{1}H NMR, ^{13}C NMR, HSQC, and HMBC. In the ^{1}H and ^{13}C NMR spectra of LYTP-3 (Figs. 8a-b), the proton signals between δ 3.30–5.50 and the carbon signals between δ 55–110 were in the characteristic regions of polysaccharides[18]. The signal at δ 174.81 and 179.61 in the ^{13}C NMR spectrum confirmed the existence of uronic acid, and δ 16.65 and 16.88 belonged to the C6 signal peak of Rha in the ^{13}C NMR spectrum[33]. After further analysis of the anomeric regions in the ^{1}H-^{1}H COSY and HSQC spectra, the chemical shifts of anomeric protons/carbons for residues A, B, C, D, E, F, G, H, and I were δ 5.27/98.41, 5.04/97.77, 4.98/97.75, 4.74/100.78, 4.65/103.70, 4.63/103.70, 4.51/102.82, 4.47/103.71, and 4.41/103.71 , respectively This indicates that residues A–C presented α configurations and D–I presented β configurations[33]. These distributions were consistent with previous methylation results[34-35].

^{1}H-^{1}H COSY spectrum generally reflects the coupling relationship between adjacent hydrocarbons (Fig. 8c). For residue A, the signals for H–2 to H–6 were deduced to be δ 4.12, 3.91, 3.51, 3.77 and 1.25. The chemical shifts for C-2 to C-6 were obtained by direct C–H correlations in the HSQC spectrum (Fig. 8d) as δ 70.21, 72.13, 69.43, 72.13, and 16.65. On comparing with literature, residue A could be identified as 1,2,4-α-*L*-Rha*p*[36]. Accordingly, residues B–I could be determined as 1,4-α-*D*-Gal*p*, 1,6-α-*D*-Glc*p*, 1,3,6-β-*D*-Man*p*, T-β-*D*-Gal*p*, 1,4-β-*D*-Gal*p*A-6-*O*-Ac, 1,6-β-*D*-Gal*p*A, T-β-*D*-Man*p,* and 1, 2-β-*L*-Rha*p* respectively[37-41]. Surprisingly, 1,6-*D*-Gal*p* and 1,3,6-*D*-Glc*p* were not detected, possibly because of their low content. All chemical shifts for protons/carbons in residues A–I are listed in Table S3.

To deduce the sequence of the glycosyl residues of LYTP-3, the HMBC spectrum was depicted in Fig. 8e. H-1 of 1,2,4-α-*L*-Rha*p* (A) correlated with C-4 of 1,4-α-*D*-Gal*p* (B). H-1 of 1,4-α-*D*-Gal*p* (B) correlated with C-6 of 1,6-α-*D*-Glc*p* (C). H-1 of 1,6-α-*D*-Glc*p* (C) has a strong correlation with C-2 of 1,2,4-α-*L*-Rha*p* (A) and C-6 of 1,3,6-β-*D*-Man*p* (D). H-1 of 1,3,6-β-*D*-Man*p* (D) correlated with C-2 of 1,2,4-α-*L*-Rha*p* (A). H-1 of T-Gal*p* (E) correlated with C-4 of 1,4-α-*D*-Gal*p* (B). H-1 of 1,4-β-*D*-Gal*p*A (F) correlated with C-2 of 1,2-β-*L*-Rha*p* (I), and H-6 of 1,4-β-*D*-Gal*p*A-6-*O*-Ac (F) was linked to an acetyl. H-1 of 1,6-β-*D*-Gal*p*A (G) and β-*D*-Man*p* (H) correlated with C-2 of 1,2,4-α-*L*-Rha*p* (A). H-1 of 1,2-β-*L*-Rha*p* (I) correlated with C-3 of 1,3,6-β-*D*-Man*p* (D)[15,32,42]. Based on these correlations, it can be concluded that the backbone of LYTP-3 was mainly composed of 1,4-α-*D*-Gal*p*, 1,6-α-*D*-Glc*p*, and 1,2,4-α-*L*-Rha*p*, which branched at the C-4 of 1,2,4-α-*L*-Rha*p* (Fig. 8f).

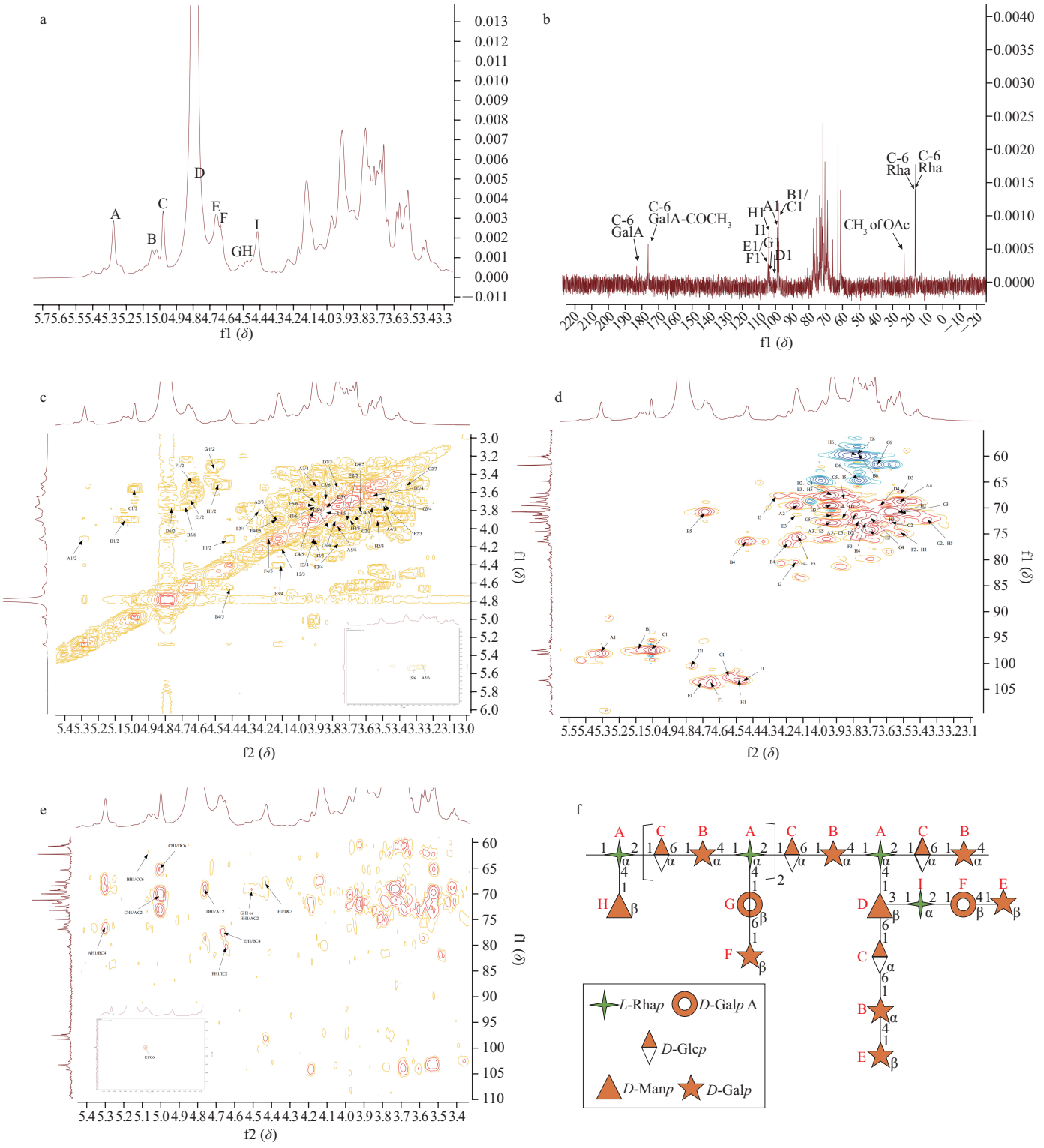

Fig. 8 NMR spectra of LYTP-3. (a) ^{1}H NMR, (b) ^{13}C NMR, (c) COSY, (d) HSQC, (e) HMBC, and (f) the proposed structures of the repeating unit of the LYTP-3.

4. Discussion

There is an inextricable correlation between dysbiosis of the gut microbiota and the occurrence and development of T2DM[43]. The gut microbiota composition in individuals with T2DM differs significantly from that of healthy individuals, with one of the most notable changes being in the ratio of Firmicutes to Bacteroidetes. Gut microbiota can affect the development of T2DM through diverse pathways, including the regulation of IR, promotion of energy metabolism, and modulation of the immune system. Many studies have reported that polysaccharides, as prebiotics, can restructure the gut microbiota and ameliorate T2DM[8,44-45].

In this study, we employed a T2DM mouse model induced by a combination of a high-fat diet and STZ to screen for bioactive compounds in LYT extract. Among these, the polysaccharide component LYTP-3 was identified as having the most pronounced hypoglycemic effects. LYTP-3 demonstrated a notable capacity to ameliorate the dysregulation of glucose and lipid metabolism in T2DM mice. Its efficacy was comparable to that of metformin and outperformed that of most previously examined polysaccharides. Surprisingly, LYTP-3 significantly boosted HDL levels in mouse serum, with efficacy comparable to that of metformin. This suggests that LYTP-3 improves T2DM by enhancing HDL levels, thereby promoting cholesterol efflux. Moreover, LYTP-3 substantially enhanced the diversity of gut microbiota. While earlier research primarily focused on the impact of polysaccharides at the phylum and genus levels, our study used metagenomic analysis to assess the influence of LYTP-3 on the gut microbiota at the species level. Our findings revealed a higher abundance of s_*Clostridium*_sp_CAG:557, Lachnospiraceae_bacterium, and s_bacterium J10(2018) and a low levels of Lachnospiraceae_bacterium_A4 and s_bacterium_0.1xD8-71 in T2DM mice, with LYTP-3 intervention effectively reversing this imbalance. Lachnospiraceae_bacterium_A4 is a specific anaerobic bacterium found in the gut[46]. Limited research exists on Lachnospiraceae_bacterium_A4. Some studies have suggested that it has potential anti-inflammatory[47-48], anti-constipation[46], and anti-colorectal cancer effects[49]. Spearman correlation analysis indicated that Lachnospiraceae_bacterium_A4 was negatively correlated with FBG, FINS, HbA1C, and HOMA-IR and was significantly enriched after LYTP-3 intervention. KEGG pathway analysis suggested that ABC transporters play a pivotal role in the LYTP-3 treatment of T2DM. ABCA1 and ABCG1 are members of the ABC gene superfamily and are responsible for cholesterol transport and HDL-C biosynthesis[50]. Glucose-stimulated insulin secretion (GSIS) reduction, accompanied by cholesterol accumulation in the islets, is considered a risk factor for glucose intolerance, leading to diabetes[51]. Here, we discovered that LYTP-3 can activate the cholesterol efflux pathway, LXRα-ABCA1/ABCG1, a process that depends on the presence of the intestinal microbiota. Among the strains tested, Lachnospiraceae_bacterium_A4 was the only strain that showed a significant negative correlation with T2DM, both before and after antibiotic cocktail therapy. Furthermore, the abundance of Lachnospiraceae_bacterium_A4 was also significantly positively correlated with the expression levels of the LXRα-ABCA1/ABCG1 pathway proteins. Collectively, these results suggest that Lachnospiraceae_bacterium_A4 may be a target strain for the treatment of T2DM by LYTP-3.

To further elucidate the molecular mechanism by which LYTP-3 improves T2DM, we predicted its molecular structure. LYTP-3 was mainly composed of 1,4-*α*-*D*-Gal*p*, 1,6-*α*-*D*-Glc*p*, and 1,2,4-*α*-*L*-Rha*p*, which branched at the C-4 of 1,2,4-*α*-*L*-Rha*p*. It is well known that the biological activity of polysaccharides is determined by their molecular structure[14]. The unique molecular structure of LYTP-3 is remarkably different from that of tea polysaccharides reported in previous studies[15]. The key distinction is the extremely complex branching structure of LYTP-3, which may be the primary reason for its remarkable biological activity. The larger the molecular weight of a polysaccharide, the higher its resistance to digestion[52]. The high molecular weight (7.22×10^5 Da) of LYTP-3 ensures its ability to exhibit prebiotic properties.

Overall, we extracted a homogeneous polysaccharide, LYTP-3, from LYT that exhibited remarkable antidiabetic activity. LYTP-3 activates the LXRα-ABCA1/ABCG1 pathway by regulating the dysbiosis of the gut microbiota in T2DM mice, thereby improving glucose and lipid metabolic disorders. Our findings hold significant promise for advancing T2DM treatment. LYTP-3 has emerged as a potential groundbreaking dietary approach for managing T2DM, and merits extensive validation in a larger cohort of T2DM patients.

Nonetheless, our study had inherent limitations. While we scrutinized the molecular structure and antidiabetic activity of LYTP-3, the intricate nature of its structure hindered a comprehensive exploration of its structure-activity relationship. Further research is imperative to elucidate the role of the Lachnospiraceae_bacterium_A4 in this context. Additionally, studies must be undertaken to understand how LYTP-3 stimulates the LXRα-ABCA1/ABCG1 pathway *via* Lachnospiraceae_bacterium_A4. Addressing these pivotal questions in future studies will pave the way for the clinical application of LYTP-3.

Conflicts of interest

The authors declare that they have no competing financial interests or personal relationships that may have influenced the work reported in this study.

Acknowledgements

The work was supported by the Open Fund of National Key Laboratory for Tea Plant Germplasm Innovation and Resource Utilization (NKLTOF20240118) and the Chen Yan Expert Workstation of Yunnan Province (202305 AF150182).

Data availability

The datasets utilized and analyzed during this investigation are available upon reasonable request from the corresponding author.

Appendix A. Supplementary data

Supplementary data associated with this article can be found, in the online version, at http://doi.org/10.26599/FSHW.2024.9250438.

References

[1] K.L. Ong, L.K. Stafford, S.A. McLaughlin, et al., Global, regional, and national burden of diabetes from 1990 to 2021, with projections of prevalence to 2050: a systematic analysis for the global burden of disease study 2021, Lancet 402 (2023) 203-234. https://doi.org/10.1016/S0140-6736(23)01301-6.

[2] S. Rossboth, M. Lechleitner, W. Oberaigner, Risk factors for diabetic foot complications in type 2 diabetes—a systematic review, Endocrinol. Diabetes Metab. 4 (2021) e00175. https://doi.org/10.1002/edm2.175.

[3] Y.H. Wong, S.H. Wong, X.T. Wong, et al., Genetic associated complications of type 2 diabetes mellitus, Panminerva. Med. 64 (2022) 274-288. https://doi.org/10.23736/S0031-0808.21.04285-3.

[4] C.M. Díaz-Perdigones, A. Muñoz-Garach, M.D. Álvarez-Bermúdez, et al., Gut microbiota of patients with type 2 diabetes and gastrointestinal intolerance to metformin differs in composition and functionality from tolerant patients,

Biomed. Pharmacother. 145 (2022) 112448. https://doi.org/10.1016/j.biopha.2021.112448.

[5] M.S. Akhter, P. Uppal, Toxicity of metformin and hypoglycemic therapies, Adv. Chronic Kidney D. 27 (2020) 18-30. https://doi.org/10.1053/j.ackd.2019.08.004.

[6] X. Chen, C. Chen, X. Fu, *Dendrobium officinale* polysaccharide alleviates Type 2 diabetes mellitus by restoring gut microbiota and repairing intestinal barrier via the LPS/TLR4/TRIF/NF-kB Axis. J. Agr. Food Chem. 71 (2023) 11929-11940. https://doi.org/10.1021/acs.jafc.3c02429.

[7] Y. Sun, Q. Nie, S. Zhang, et al., *Parabacteroides distasonis* ameliorates insulin resistance *via* activation of intestinal GPR109a, Nat. Commun. 14 (2023) 7740. https://doi.org/10.1038/s41467-023-43622-3.

[8] S. Chen, F. Zeng, W. Fu, et al., White hyacinth bean polysaccharide ameliorates diabetes *via* microbiota-gut-brain axis in type 2 diabetes mellitus rats, Int. J. Biol. Macromol. 253 (2023) 127307. https://doi.org/10.1016/j.ijbiomac.2023.127307.

[9] M. Yang, J. Lv, J. Yang, et al., Effects of *Codonopsis pilosula* crude polysaccharides by hypoglycemic and modulating gut microbiome in a high-fat diet and streptozotocin-induced mouse model of T2DM, J. Funct. Foods. 111 (2023) 105893. https://doi.org/10.1016/j.jff.2023.105893.

[10] Z. Bai, X. Huang, G. Wu, et al., Polysaccharides from small black soybean alleviating type 2 diabetes *via* modulation of gut microbiota and serum metabolism, Food Hydrocoll. 141 (2023) 108670. https://doi.org/10.1016/j.foodhyd.2023.108670.

[11] J. Zhou, L. Zhang, Q. Meng, et al., Roasting improves the hypoglycemic effects of a large-leaf yellow tea infusion by enhancing the levels of epimerized catechins that inhibit alpha-glucosidase, Food Funct. 9 (2018) 5162-5168. https://doi.org/10.1039/c8fo01429a.

[12] N. Xu, J. Chu, M. Wang, et al., Large yellow tea attenuates macrophage-related chronic inflammation and metabolic syndrome in high-fat diet treated mice, J. Agr. Food Chem. 66 (2018) 3823-3832. https://doi.org/10.1021/acs.jafc.8b00138.

[13] C. Zhou, Y. Huang, J. Chen, et al., Effects of high-pressure homogenization extraction on the physicochemical properties and antioxidant activity of large-leaf yellow tea polysaccharide conjugates, Process Biochem. 122 (2022) 87-94. https://doi.org/10.1016/j.procbio.2022.09.020.

[14] H. Chen, Y. Huang, C. Zhou, et al., Effects of ultra-high pressure treatment on structure and bioactivity of polysaccharides from large leaf yellow tea, Food Chem. 387 (2022) 132862. https://doi.org/10.1016/j.foodchem.2022.132862.

[15] H. Wang, S. Xu, D. Li, et al., Structural characterization and macrophage polarization-modulating activity of a novel polysaccharide from large yellow tea, J. Agr. Food Chem. 70 (2022) 12565-12576. https://doi.org/10.1021/acs.jafc.2c05593.

[16] X. Wang, N. Zhang, H. Zhang, et al., Characterization, antioxidant and hypoglycemic activities of an acid-extracted tea polysaccharide, Int. J. Polym. Anal. Ch. 27 (2022) 195-204. https://doi.org/10.1080/1023666X.2022.2043536.

[17] E.G. Shakhmatov, V.A. Belyy, E.N. Makarova, Structure of acid-extractable polysaccharides of tree greenery of *Picea abies*, Carbohyd. Polym. 199 (2018) 320-330. https://doi.org/10.1016/j.carbpol.2018.07.027.

[18] N. Zhang, H. Ma, Z. Zhang, et al., Characterization and immunomodulatory effect of an alkali-extracted galactomannan from *Morchella esculenta*, Carbohyd. Polym. 278 (2022) 118960. https://doi.org/10.1016/j.carbpol.2021.118960.

[19] M. Dubois, K.A. Gilles, J.K. Hamilton, et al., Colorimetric method for determination of sugar and related substances, Anal. Chem. 28 (1956) 250-256.

[20] M. Ognyanov, C.A. Remoroza, H.A. Schols, et al., Structural study of a pectic polysaccharide fraction isolated from "mountain tea" (*Sideritis scardica Griseb*.), Carbohyd. Polym. 260 (2021) 117798. https://doi.org/10.1016/j.carbpol.2021.117798.

[21] M.M. Bradford, A rapid and sensitive method for the quantitation of microgram quantities of protein utilizing the principle of protein-dye binding, Anal. Biochem. 72 (1976) 248-254. https://doi.org/10.1016/0003-2697(76)90527-3.

[22] T. Zhang, H. Liu, X. Bai, et al., Fractionation and antioxidant activities of the water-soluble polysaccharides from *Lonicera japonica* Thunb, Int. J. Biol. Macromol. 151 (2020) 1058-1066. https://doi.org/10.1016/j.ijbiomac.2019.10.147.

[23] Y. Zhang, D. Zhuang, H. Wang, et al., Preparation, characterization, and bioactivity evaluation of oligosaccharides from *Atractylodes lancea* (Thunb.) DC, Carbohyd. Polym. 277 (2022) 118854. https://doi.org/10.1016/j.carbpol.2021.118854.

[24] Z. Cai, W. Li, S. Mehmood, et al., Structural characterization, *in vitro* and *in vivo* antioxidant activities of a heteropolysaccharide from the fruiting bodies of *Morchella esculenta*, Carbohyd. Polym. 195 (2018) 29-38. https://doi.org/10.1016/j.carbpol.2018.04.069.

[25] T. Xia, C. Liu, Y. Hu, et al., Coix seed polysaccharides alleviate type 2 diabetes mellitus *via* gut microbiota-derived short-chain fatty acids activation of IGF1/PI3K/AKT signaling, Food Res. Int. 150 (2021) 110717. https://doi.org/10.1016/j.foodres.2021.110717.

[26] Q. Zheng, Y. Zheng, R. Jia, et al., Fucus vesiculosus polysaccharide alleviates type 2 diabetes in rats *via* remodeling gut microbiota and regulating glycolipid metabolism-related gene expression, Int. J. Biol. Macromol. 248 (2023) 126504. https://doi.org/10.1016/j.ijbiomac.2023.126504.

[27] B. Chen, L. Sun, G. Zeng, et al., Gut bacteria alleviate smoking-related NASH by degrading gut nicotine, Nature 610 (2022) 562-568. https://doi.org/10.1038/s41586-022-05299-4.

[28] F. Huang, X. Zheng, X. Ma, et al., Theabrownin from Pu-erh tea attenuates hypercholesterolemia *via* modulation of gut microbiota and bile acid metabolism. Nat. Commun. 10 (2019) 4971. https://doi.org/10.1038/s41467-019-12896-x.

[29] Z. Wang, L. Ding, J. Liu, et al., Allicin ameliorates glucose and lipid metabolism *via* modulation of gut microbiota and bile acid profile in diabetic rats, J. Funct Foods. 111 (2023) 105899. https://doi.org/10.1016/j.jff.2023.105899.

[30] Y. Zhang, Y. Peng, L. Zhao, et al., Regulating the gut microbiota and SCFAs in the faeces of T2DM rats should be one of antidiabetic mechanisms of mogrosides in the fruits of *Siraitia grosvenorii*, J. Ethnopharmacol. 274 (2021) 114033. https://doi.org/10.1016/j.jep.2021.114033.

[31] Y. Zhang, J. Wang, W. Ge, et al., Camel milk peptides alleviate hyperglycemia by regulating gut microbiota and metabolites in type 2 diabetic mice, Food Res. Int. 173 (2023) 113278. https://doi.org/10.1016/j.foodres.2023.113278.

[32] M. Liu, Z. Gong, H. Liu, et al., Structural characterization and anti-tumor activity *in vitro* of a water-soluble polysaccharide from dark brick tea, Int. J. Biol. Macromol. 205 (2022) 615-625. https://doi.org/10.1016/j.ijbiomac.2022.02.089.

[33] P. Jiang, X. Ji, J. Xia, et al., Structure and potential anti-fatigue mechanism of polysaccharides from *Bupleurum chinense* DC, Carbohyd. Polym. 306 (2023) 120608. https://doi.org/10.1016/j.carbpol.2023.120608.

[34] Y. Jiang, Z. Shang, X. Lv, et al., Structure elucidation and antitumor activity of a water soluble polysaccharide from *Hemicentrotus pulcherrimus*. Carbohyd. Polym. 292 (2022) 119718. https://doi.org/10.1016/j.carbpol.2022.119718.

[35] Y. Fu, C. Li, X. Peng, et al., Polysaccharides from *Aconitum carmichaelii* leaves: structure, immunomodulatory and anti-inflammatory activities, Carbohyd. Polym. 291 (2022) 119655. https://doi.org/10.1016/j.carbpol.2022.119655.

[36] Z. Lin, T. Li, Q. Yu, et al., Structural characterization and *in vitro* osteogenic activity of ABPB-4, a heteropolysaccharide from the rhizome of *Achyranthes bidentata*, Carbohyd. Polym. 259 (2021) 117553. https://doi.org/10.1016/j.carbpol.2020.117553.

[37] R. Guo, J. Zhang, X. Liu, et al., Pectic polysaccharides from Biluochun tea: a comparative study in macromolecular characteristics, fine structures and radical scavenging activities *in vitro*, Int. J. Biol. Macromol. 195 (2022) 598-608. https://doi.org/10.1016/j.ijbiomac.2021.12.004.

[38] Y. Cui, Y. Chen, S. Wang, et al., Purification, structural characterization and antioxidant activities of two neutral polysaccharides from persimmon peel, Int. J. Biol. Macromol. 225 (2023) 241-254. https://doi.org/10.1016/j.ijbiomac.2022.10.257.

[39] T. Zhao, G. Mao, W. Feng, et al., Isolation, characterization and antioxidant activity of polysaccharide from *Schisandra sphenanthera*, Carbohyd. Polym. 105 (2014) 26-33. https://doi.org/10.1016/j.carbpol.2014.01.059.

[40] X. Cheng, S. Shi, J. Su, et al., Structural characterization of a heteropolysaccharide from fruit of *Chaenomelese speciosa* (Sweet) Nakai

and its antitumor activity, Carbohyd. Polym. 236 (2020) 116065. https://doi.org/10.1016/j.carbpol.2020.116065.

[41] L. Yang, C. Zi, D. Chen, et al., Target acquisition of anti-aging manno-oligosaccharide that triggers ECM process *via* TGF-β/Smads-SIRT1 signalling pathway. Carbohyd. Polym. 302 (2023) 120380. https://doi.org/10.1016/j.carbpol.2022.120380.

[42] S. Zhang, Y. Li, Z. Li, et al., Structure, anti-tumor activity, and potential anti-tumor mechanism of a fungus polysaccharide from *Fomes officinalis*, Carbohyd. Polym. 295 (2022) 119794. https://doi.org/10.1016/j.carbpol.2022.119794.

[43] M. Gurung, Z. Li, H. You, et al., Role of gut microbiota in type 2 diabetes pathophysiology, Ebiomedicine 51 (2020) 102590. https://doi.org/10.1016/j.ebiom.2019.11.051.

[44] Y. Yao, L. Yan, H. Chen, et al., *Cyclocarya paliurus* polysaccharides alleviate type 2 diabetic symptoms by modulating gut microbiota and short-chain fatty acids, Phytomedicine 77 (2020) 153268. https://doi.org/10.1016/j.phymed.2020.153268.

[45] Y.A. Kim, J.B. Keogh, P.M. Clifton, Probiotics, prebiotics, synbiotics and insulin sensitivity, Nutr. Res. Rev. 31 (2018) 35-51. https://doi.org/10.1017/S095442241700018X.

[46] H. Yang, C. Wu, L. Chen, et al., *A. macrocephala* polysaccharide induces alterations to gut microbiome and serum metabolome in constipated mice, Microb. Pathogenesis. 178 (2023) 106084. https://doi.org/10.1016/j.micpath.2023.106084.

[47] C. Manichanh, L. Rigottier-Gois, E. Bonnaud, et al., Reduced diversity of faecal microbiota in Crohn's disease revealed by a metagenomic approach, Gut 55 (2006) 205-211. https://doi.org/10.1136/gut.2005.073817.

[48] D.N. Frank, A.A. St, R.A. Feldman, et al., Molecular-phylogenetic characterization of microbial community imbalances in human inflammatory bowel diseases, PNAS. 104 (2007) 13780-13785. https://doi.org/10.1073/pnas.0706625104.

[49] S.G. Daniel, C.L. Ball, D.G. Besselsen, et al., Functional changes in the gut microbiome contribute to transforming growth factor *β*-deficient colon cancer, Msystems 2 (2017). https://doi.org/10.1128/mSystems.00065-17.

[50] M.M. Hasan, M.B. Hosen, M.M. Rahman, et al., Association of ATP binding cassette transporter 1 (ABCA 1) gene polymorphism with type 2 diabetes mellitus (T2DM) in Bangladeshi population, Gene 688 (2019) 151-154. https://doi.org/10.1016/j.gene.2018.12.003.

[51] M. Vergeer, L.R. Brunham, J. Koetsveld, et al., Carriers of loss-of-function mutations in ABCA1 display pancreatic beta-cell dysfunction, Diabetes Care 33 (2010) 869-874. https://doi.org/10.2337/dc09-1562.

[52] M. Chen, X. Chen, Y. Guo, et al., Effect of *in vitro* digestion and fermentation of kiwifruit pomace polysaccharides on structural characteristics and human gut microbiota, Int. J. Biol. Macromol. 253 (2023) 127141. https://doi.org/10.1016/j.ijbiomac.2023.127141.